Tectonophysics 706–707 (2017) 91–102

Contents lists available at ScienceDirect

Tectonophysics

journal homepage: www.elsevier.com/locate/tecto

An extending island arc: The case of Kamchatka

Andrey Kozhurin [a,b], Egor Zelenin [b,*]

[a] Institute of Volcanology and Seismology, Piip Blvd 9, Petropavlovsk-Kamchatsky, Russia,
[b] Geological Institute, Pyzhevsky per. 7, Moscow, Russia

ARTICLE INFO

Article history:
Received 22 November 2016
Received in revised form 10 March 2017
Accepted 1 April 2017
Available online 5 April 2017

Keywords:
Island arc
Trench retreat
Normal faulting
Low angle faults
Extension rate
Kamchatka

ABSTRACT

We report a first estimate of the extension rate of the onshore Kamchatka island arc, it central wider part. This average rate is 17 ± 3 mm/yr over mid-late Quaternary time. The extension is absorbed by slip on major normal active faults of Central Kamchatka, and graben-producing faulting in its volcanic belt. Probable extension of the underwater portion of the arc, its rate remaining unknown, may add up to the total value. The onshore extension rate, established by remote fault scarp measurements on DEMs resembles the numerical modelling estimate of Schellart et al. (2007), suggesting that the primary driving force responsible for the extension at Kamchatka is slab and trench retreat.

1. Introduction

The deformation of an island arc is governed by two main factors. The first factor is the relative angle of convergence between the oceanic plate and the island arc. For example, oblique convergence can produce a component of lateral along-arc movement in the arc, as first described by Fitch (1972). The second factor is the proximity of the arc to the lateral edge of the subducting slab: the closer the arc is to the edge, the higher the possibility that the arc will extend in the direction of the retreating slab (Schellart et al., 2007). In any case, the rate of tectonic motion within an arc (either arc-normal shortening or extension, with or without an along-arc component) can be used to estimate the proportion of relative convergence accommodated by arc deformation, and the relative degree of coupling between the downgoing and overriding plates.

Published estimates suggest that approximately half of the island arcs around the world, including Kamchatka (Acocella and Funiciello, 2010), are extending by approximately 70% of their total length (Schellart et al., 2008). The Peninsula of Kamchatka lies above the northern edge of the subducted portion of the Pacific Plate, and currently undergoes extension, as evidenced by its basin-and-range topography and pervasive normal faulting in the northern two-thirds of the peninsula (Fig.1). Shantser (1979) described this extension as "a collapse of a pre-existing orogen". This description is quite appropriate because the ongoing extension, after some period of relative quiescence, followed collision-related shortening in Kamchatka caused by the docking of the Paleocene-Eocene Kronotsky arc, with the most recent thrusting deformation at approximately 2 Ma (Lander and Shapiro, 2007). Extension was at first slow, and the topography of Central Kamchatka was likely gentle. Only finely laminated lacustrine sediments (Brunhes Chron) accumulated in its axial region, which subsequently evolved into the Central Kamchatka Depression. Vertical movement between the depression and the high-elevation Eastern Ranges, coupled with arc-normal extension, accelerated in Kamchatka in the middle Pleistocene, and it is marked by the first appearance of coarse gravel-bearing material in the depression (Braitseva et al., 1968; Braitseva et al., 2005).

Based on numerical modelling, Schellart et al. (2007) found that Kamchatka may be extending oceanward at a rate of 28 mm/yr. In contrast, Acocella and Funiciello (2010), with reference to Kozhurin personal communication, reported that 10 ± 5 mm/yr is the likely rate of extension in Kamchatka. These estimates represent tempting targets to verify using ground-based data.

Two faults zones accommodating arc-normal extension are recognized in Central Kamchatka (Fig. 1). The first is the East Kamchatka Fault Zone (EKFZ), which includes the normal faults (naming conventions after Kozhurin et al., 2006) that divide the asymmetric Central Kamchatka Depression (CKD) from the Eastern Ranges to the east. Most of the faults dip north-west and produce an approximately 1-km-high faceted slope (Fig. 2). To the east, another zone comprises segmented en-échelon systems of grabens and nested grabens along the axis of the Eastern Volcanic Front and may therefore be termed volcano-tectonic deformation. This area was first mapped by Legler (Legler and Parfenov, 1979), who defined it as the "Volcanic Opening," meaning that grabens may have formed due to the splitting forces generated by

* Corresponding author.
E-mail addresses: anivko@yandex.ru (A. Kozhurin), egorzelenin@mail.ru (E. Zelenin).

http://dx.doi.org/10.1016/j.tecto.2017.04.001
0040-1951/

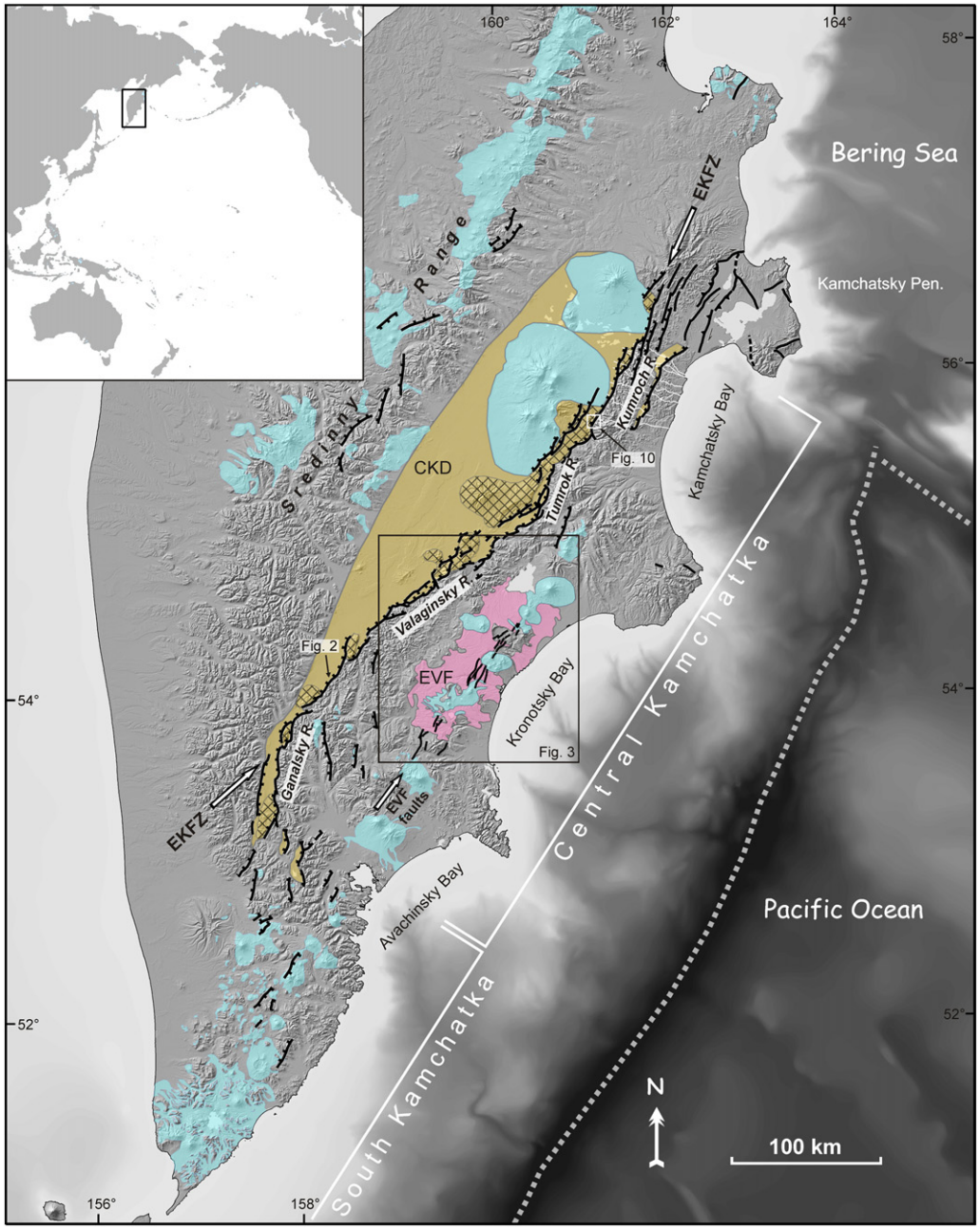

Fig. 1. Active faulting and late Quaternary volcanism of Kamchatka. Faults are black lines with hatches for normal faults, triangles for reverse and thrust faults, and one-sided arrows for strike-slip faults. The larger, open arrow points at the East Kamchatka Fault Zone (EKFZ) and the smaller arrow points at the system of normal faults in the Eastern Volcanic Front (EFV). The yellow-filled, cross-hatched areas along the east margin of the Central Kamchatka Depression (CKD) are blocks of intermediate topographic height (i.e., half-elevated or half-downthrown). Blue areas are those covered by upper Pleistocene-Holocene volcanic deposits, shown as in Ponomareva et al. (2007) and in GIS "Holocene volcanism of Kamchatka". The purple-colored area is Pleistocene ignimbrite sheets of the Eastern Volcanic Front. Thin white lines in the Kumroch Range are lines of hypsometric profiles used for measuring block tilt (see text for details). Dotted white lines east of Kamchatka are axes of oceanic trenches. Bathymetry after Seliverstov, 2009.

magma intruding into the crust. Later, Florensky and Trifonov (1985) determined that the entire system of grabens is a "channel" that facilitates the transport of magma through the crust. Several relatively short normal faults have also been discovered west of the CKD in the Sredinny Range. These faults are poorly expressed in topography and are obviously extremely slow moving. In addition to the faults zones already described, reverse and strike-slip faults predominate north of Central Kamchatka in the Kamchatsky Peninsula (see Fig. 1). This difference in faulting marks a distinctly different tectonic setting caused by the collision of the western Aleutians with Kamchatka (Kozhurin et al., 2014). Transition of the kinematics, from extension in Central Kamchatka to collisional shortening in the north, remains poorly studied.

The rate at which onshore Central Kamchatka has been extending since the middle Quaternary may be roughly determined based on the sum of the arc-normal components of movement on the EKFZ and on the set of grabens in the East Volcanic Front. Quantifying extension in a rift-perpendicular direction by aggregating fault displacements produced at, or near, the ground surface is a standard technique used on rift-systems globally (e.g., Villamor and Berryman, 2001; Nicol et al., 2006; Begg and Mouslopoulou, 2010; Giba et al., 2010; Mouslopoulou et al., 2012). To date, no one has reported, based on filed measurements, the rates with which the Kamchatka island arc is extending. Legler and Parfenov (1979) attempted to estimate the rate of volcano-tectonic normal faulting by assuming an average normal fault dip of 60° and an

Fig. 2. Faceted spurs, Ganalsky Range. View to SE (see Fig. 1 for location).

average thickness of dykes observed in outcrops of 2 to 3 m. The calculated value for the average rate of extension was 3 mm/yr and was surprisingly uniform over periods since 10, 30 and 100 ka. Nevertheless, no details of their estimates (e.g., number of faults or individual vertical net offsets) were reported.

This paper represents the first attempt to derive an extension rate based on geomorphological data and, partly, trench data. We focused on two segments of the East Volcanic Front (EVF), where faults are numerous and well expressed topographically, and on two segments of the EKFZ (Fig. 1). The studied features in the EVF are the faults in the Shirokoye Plateau, located immediately south of the late Pleistocene Uzon-Geyzernaya caldera depression, and the Semiachik Plateau, located just south of the Pleistocene Bolshoi Semiachik volcano, both of which are mantled by late Pleistocene ignimbrites (Figs. 1 and 3). To derive the necessary parameters for estimating extension rates in the EKFZ, we focused on two localities, one close to the northern termination of the EKFZ (Fig. 10, see Fig. 1 for location) and the other just west of the two plateaus (Fig. 11, see Fig. 3 for location).

2. Methods

Determining the lateral extensional component of slip on a fault may be possible if its 3D geometry is known. A fault plane can be planar, listric, ramp-flat, among other shapes, and variations in its geometry strongly influence estimates of the extensional component. When the geometry of a fault plane cannot be determined in detail, the dip of the fault plane across some depth interval (the greater depth more accurate the dip estimate) is a primary and essential proxy.

In densely vegetated terrain, such as Kamchatka, where outcrops are rare, two approaches are possible: 1) the fault dip can be measured directly in a trench wall; 2) an average fault dip can be determined based on the bending of the fault line as it crosses rugged terrain. The second approach is preferable, as a shallow or listric fault plane may become nearly vertical just beneath the ground surface due to, for example, toppling. Thus, trench data, although valuable, may be misleading for estimating fault plane geometry and may lead to incorrect conclusions, e.g., that a fault plane is planar and nearly vertical.

To estimate fault plane geometry, we first mapped the key normal faults in the study area. We interpreted aerial photos at various scales and satellite imagery to identify the mapview geometry of faults. We primarily used KH-9 Hexagon stereoscopic imagery (from the U.S. Geological Survey) with approximately 5-m resolution at nadir. For both aerial photos and satellite imagery, stereoscopic models were created and interpreted using Photomod 6.0 Lite software (Racurs Co., Russia).

To estimate vertical offsets on individual faults, we used the digital elevation models (DEMs) ASTER GDEM (a product of NASA and METI) and SRTM X-SAR (©DLR/ASI), both with approximately 30-m spatial resolutions. We also built a 2-m-resolution DEM covering the Shirokoye Plateau using detailed aerial photos and Agisoft Photoscan software. Due to the absence of geodetic markers on the Shirokoye Plateau, the accuracy of the detailed DEM was verified using ASTER GDEM data and Russian topographic maps at 1:100,000 scale. All of the above DEM measurements were ground-truthed during extensive fieldwork on the Kamchatka Peninsula. In addition, we also excavated two trenches, one on each of the two plateaus, to measure fault dip angles in the upper 2–3 m of the ground.

3. Faults of the East Volcanic Front

The ~130-km-long fault zone strikes ~37°NNE and consists of three distinct segments (Fig. 3): the Zhupanovsky-Karymsky segment in the south (as named by Florensky and Trifonov, 1985), the central Semiachik segment, and the Uzon segment in the north (Figs. 1 and 3). The Uzon segment includes faults on the Shirokoye Plateau, faults within the Uzon-Geyzernaya caldera depression, and faults extending to the north to the Krasheninnikov caldera. In all three segments, the faults display Pleistocene pyroclastic deposits created by caldera-forming eruptions and younger, post-caldera, deposits within the Uzon-Geyzernaya depression.

As noted earlier, the fault zone geometry varies along strike (Legler and Parfenov, 1979; Florensky and Trifonov, 1985): the fault zone gradually narrows northward from ~10 km south of the Karymsky volcano to ~2 km north of the Uzon-Geyzernaya depression. Additionally, the segments are slightly en-échelon, with a right-stepping arrangement, which Florensky and Trifonov (1985) interpreted to result from some left-lateral component of slip along the fault zone.

3.1. The Shirokoye plateau

The Shirokoye Plateau represents a fragment of an ignimbrite sheet that formed during the Uzon caldera-forming eruption (Florensky, 1984; Leonov and Grib, 2004; Bindeman et al., 2010). The plateau is flat and slightly tilted southward towards the Bolshoi Semiachik massif and is heavily faulted. We mapped 15 major faults (Fig. 4), with scarps >1 m high, using stereoscopic pairs of aerial images. Other faults are

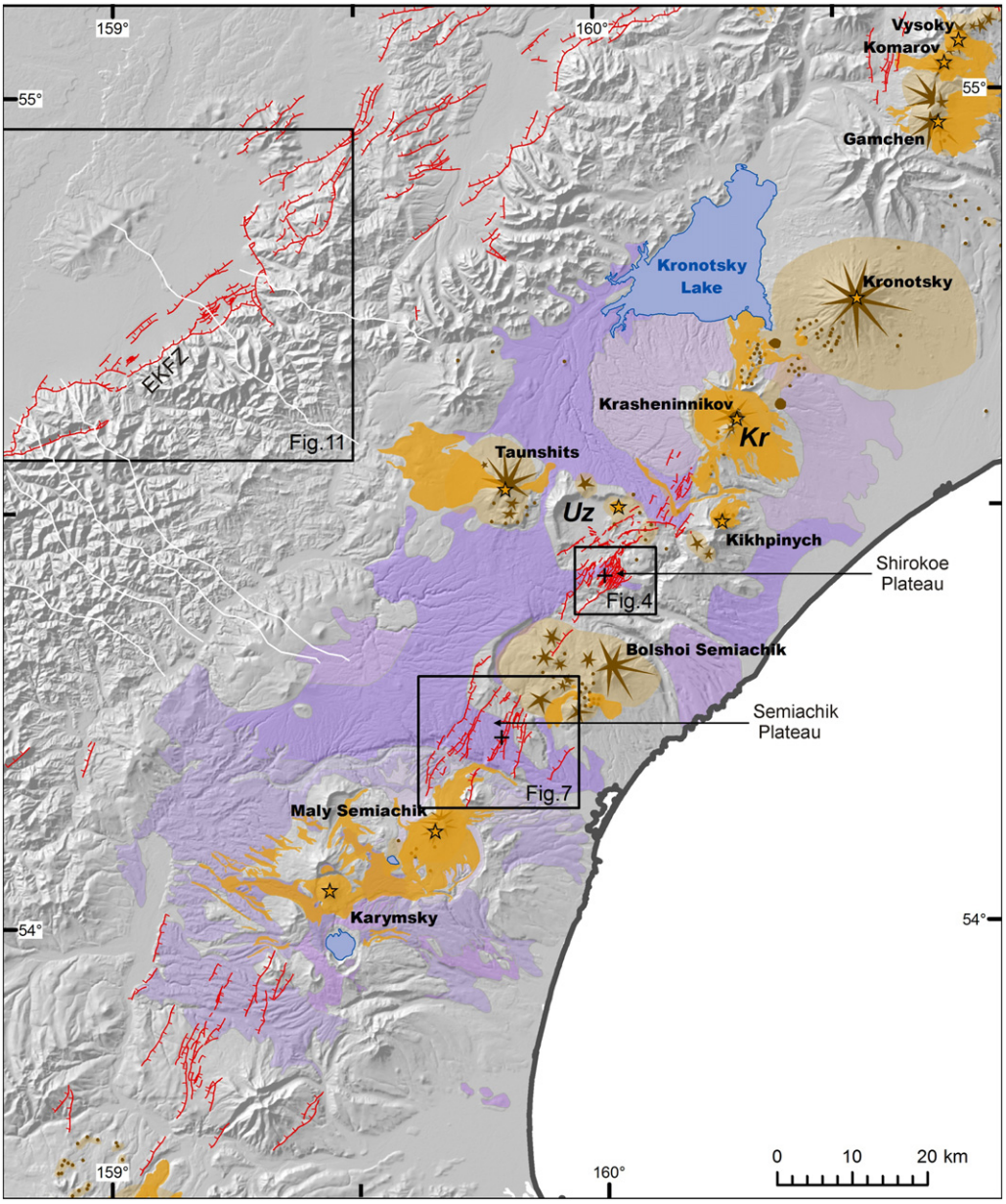

Fig. 3. Active normal faults in the Eastern Volcanic Front. Lighter and darker lilac- colored areas are individual sheets of Pleistocene ignimbrites. Light brown and orange colors mark upper Pleistocene and Holocene volcanic deposits, respectively. Red lines are normal faults in the East Volcanic Front and in the Valaginsky segment of the EKFZ (upper left corner), hatches on downthrown side. Thin white lines in the Valaginsky Range are lines of hypsometric profiles used for measuring blok tilt (see text for details). Black crosses mark the thench sites. Abbreviations: Uz = Uzon-Geyzernaya depression, Kr = Krasheninnikov caldera.

clearly visible in the imagery, but the net vertical offsets in topography are less than the vertical resolution of the DEM, which is approximately 1 m. These faults also contribute extension to the graben, but we could not assess their impact with sufficient accuracy. Most of the faults terminate within the plateau, but some were found to cross the caldera rim and extend northward into the Uzon-Geyzernaya depression. In the southern part of the study area, only one of the faults extends to the valley of the Bezymianny Creek and further south onto the slope of the late Pleistocene Bolshoi Semiachik volcano (Leonov and Grib, 2004).

Quantitative characteristics of the graben were derived from aerial orthoimagery and the Shirokoye DEM. The total vertical displacement accrued on faults in a graben-perpendicular direction was measured on topographic profiles performed on the Shirokoye DEM (Fig. 5). The measured total vertical displacement is 147 ± 9 m (13 individual fault measurements on 1-m DEM) in the northern profile A and 174 ± 8 m (11 individual fault measurements on 1-m DEM) in the southern profile B. Both values represent a minimum due to the missing faults (ground displacement < 1 m) and also because of the accuracy of errors in reconstructing the pre-deformed surfaces. To avoid overestimation of the extension rate we further used the lesser value. Both profiles yield a similar graben depth of 60–65 m.

The estimation of total extension, based on total vertical displacement, requires information on the fault dips. Therefore, we excavated and measured one of the normal fault planes, as it is exposed in a 2-m-deep trench. Immediately below the ground surface, the fault dips steeply beneath the elevated side (Fig. 6). Deeper, it curves to vertical, and at the trench bottom, it dips 60° towards the downthrown side. The reverse sense in the upper meter of soil-pyroclastic cover is apparent and may be due to mass movement down the fault scarp (Fig. 6). The major plane is accompanied in the hanging wall by antithetic faults and opening fractures, which indicate that the fault plane may have an even shallower dip at greater depth.

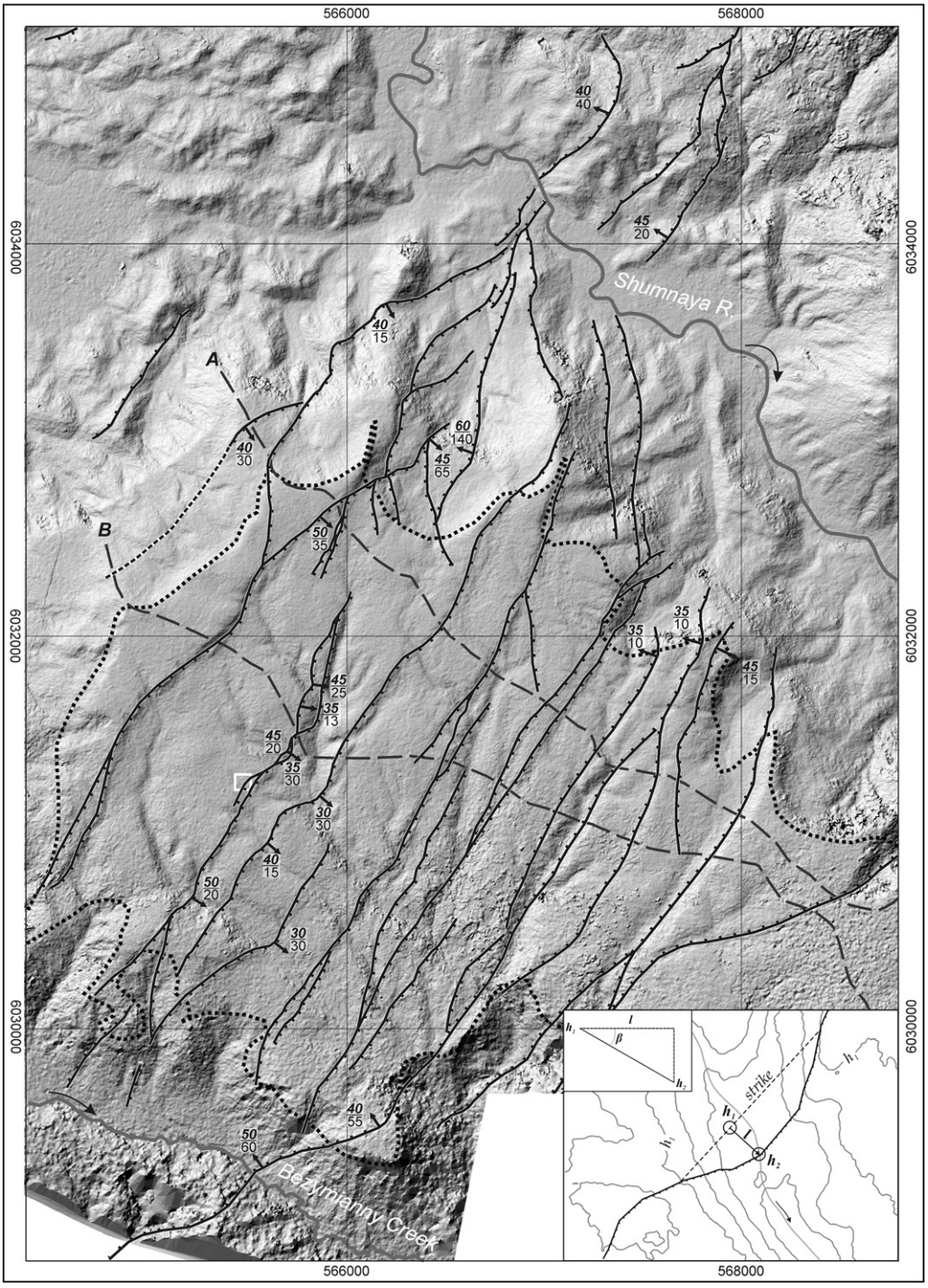

Fig. 4. Faults on the Shirokoe Plateau (for location, see Fig. 3). The background is a hill-shaded, 2-m-resolution digital elevation model of the plateau, generated by aerial images (grid marks in meters). Thick dotted line approximates the plateau edge. Solid black lines are faults, hatches on downthrown side. Two dashed lines A and B are lines of topographic profiles shown on Fig. 5. Black arrows indicate direction of fault dip, numbers are dip angle (above) and corresponding depth interval in m (below). White rectangle shows the trench site (Fig. 6). Inset illustrates procedure of fault dip (β) determination (the fault SE of the trench).

To estimate the mean dip angle from a representative number of faults, we measured bends in the faults at intersections with landforms visible on aerial imagery. However, we could not completely avoid ambiguity while tracing faults on steep slopes between plateau and river valleys. Therefore, we concentrated on measuring fault bends where they cross small creeks and hills on the plateau, which provided us with total 16 measurements (Fig. 4). Most of the measured dip angles on the plateau are in the order of 30–45°, and only one measurement (in the Bezymianny Creek valley, in the lower right corner of Fig. 4) yielded a steeper angle of ca. 50°. The maximal measured angle was 60°, located in the upper part of a southern slope in the Shumnaya valley, while the median value of dip angles was 40° ± 8°.

To calculate the total extension, we used the cumulative vertical fault displacement of 147 ± 9 m and a dip angle of 40 ± 8° (assuming a planar geometry with depth). We did not take into account opening fractures and faults with <1 m of net vertical offset. The magnitude of

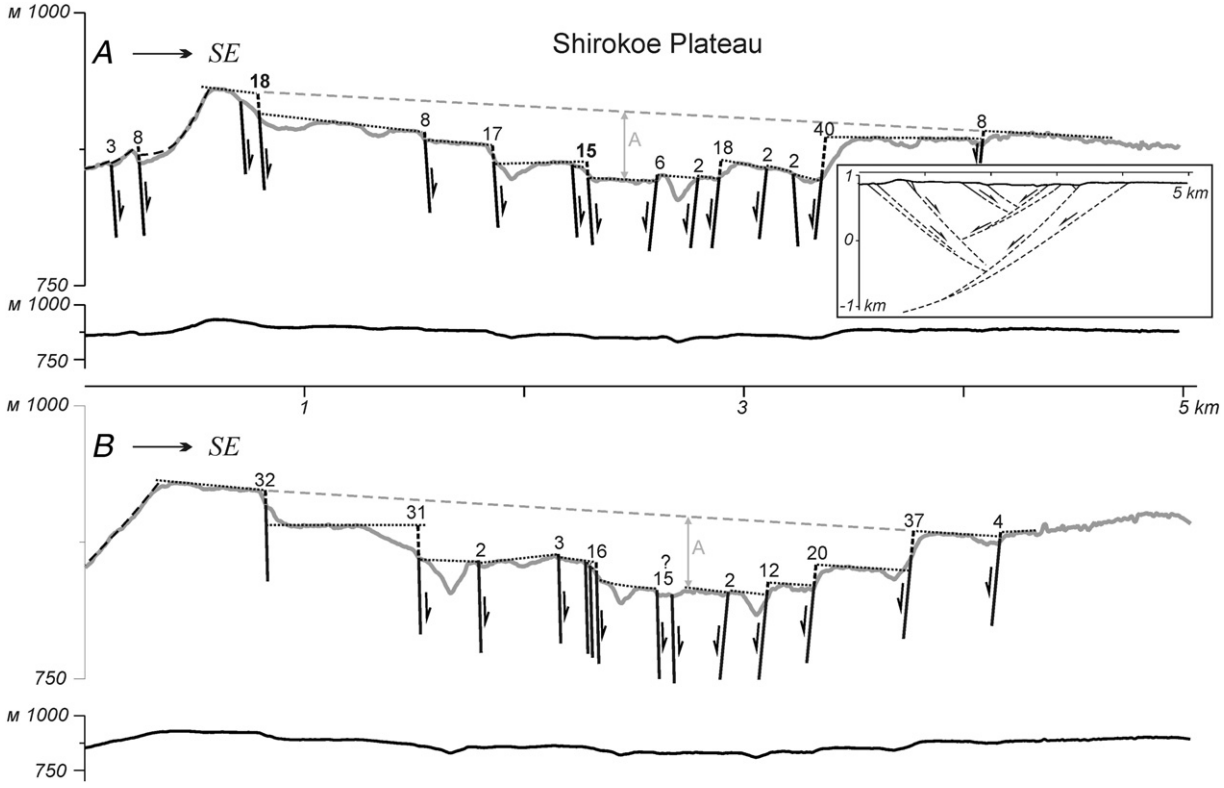

Fig. 5. Hypsometric profiles across the Shirokoe Plateau (see Fig. 4 for location), derived from the 2-m Shirokoe DEM. Lower solid black lines are profiles with no vertical exaggeration, and upper solid grey lines are 5-times vertically exaggerated. Dotted lines approximate fragments of the plateau top surface, with numbers, in meters, indicating amount of their vertical separation measured by profiles (bold where combining two neighbouring smaller vertical offsets). Sum of these values for each of the profiles is total vertical component (147 m and 174 m on A and B, respectively). Dashed grey lines show pre-faulted plateau surface, and grey "A" letters mark graben depth (61–61 m on profile A, and 64–65 m on profile B). Inset in rectangle demonstrates hypothetical cross-section of the faulted plateau based on accepted fault dips.

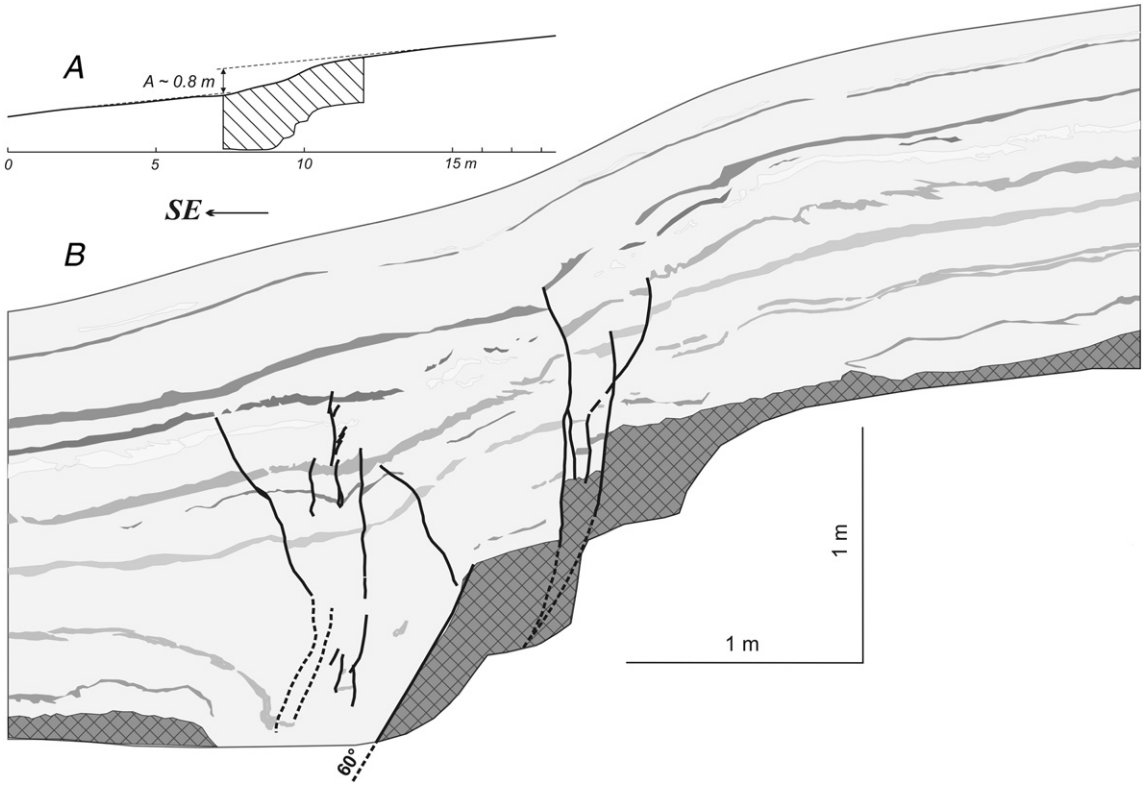

Fig. 6. Shirokoye trench south wall. A = topographic profile, hatched area is the trench extent, B = log of the southern trench wall. Solid black lines are faults (dashed where uncertain) offsetting both Holocene soil-pyroclastic sequence (upper light grey area with tephra layers) and its basement (dark grey, cross-hatched), composed of disintegrated ignimbrites. Dip of the main fault plane is indicated. Note that one-event and cumulative offsets of individual tephra layers are very small (see Section 5 for discussion).

resultant lateral extension is 175 ± 50 m, which is equal or greater than the total vertical component. The error propagation was conducted using the traditional method (e.g. Rabinovich, 2006).

The width of the graben was just 4 km, suggesting that the faulted layer is not thick. With dip angles of 40 ± 8°, the easternmost and westernmost faults meet at a depth of less than ~2.5 km below the surface. Even with the maximal measured dip angle of 60°, the brittle layer cannot be thicker than approximately 3.5 km.

3.2. Age of the Shirokoye Plateau and the average extension rate

The ignimbrites on the Shirokoe Plateau are just a small portion of the vast ignimbrite sheets that formed during the Uzon caldera-forming eruption. These ignimbrites spread to the shores of Kronoskoe Lake in the north and to the Novy Semiachik River valley, south of the Bolshoi Semiachik volcanic centre, in the south (Fig. 3). To date, two ages for this ignimbrite have been published in the literature. Florensky (1984) obtained a ^{14}C date of 39,600 ± 1000 ka by radiocarbon dating wood beneath the ignimbrite sheet close to Kronotskoe Lake. Using OxCal 4.2 (Bronk Ramsey, 2009) with the IntCal13 calibration curve (Reimer et al., 2013) we estimate the age of the ignimbrite sheet to be younger than 43,603 ± 1676 BP (2σ). In contrast, Bindeman et al. (2010) obtained an age of 278 ± 17 ka BP by Ar-Ar dating a sample from the upper of three older ignimbrite units in the southern scarp of the Shirokoye Plateau. Based on these two contrasting dates, Bindeman et al. (2010) concluded that the Uzon caldera must consist of two superimposed calderas of different ages.

The plateau is only slightly eroded and it bears no evidence of glacial modification that could have eliminated earlier erosional features. The only glacial landforms found here are several cirques that are located in the north of the plateau and that form 40 to 50 m deep "bays" cut into the plateau edge (Fig. 4). Each cirque is located between a pair of antithetic faults. Some faults extend from the plateau into the "bays" but have smaller accumulated vertical displacement than those on the plateau itself. Based on the observations above, we assume that the ~40 ka eruption mantled middle Quaternary deposits, at least on the plateau, and that the younger of the two dates most likely represents the maximum age of the plateau surface. Therefore, we attribute the vertical deformation measured on the ground surface of the plateau to have formed during the last ca. 43,000 years. With the extension of 175 ± 50 m our estimate for the extension rate is 4.0 ± 1.2 mm/yr.

3.3. The Semiachik Plateau

The Semiachik Plateau, the ignimbrite plateau between Bolshoi Semiachik and Maly Semiachik volcanoes, is also heavily faulted. To map faults on this plateau, we applied the same techniques used for the Shirokoye Plateau but used smaller-scale aerial imagery and the much less precise SRTM X-SAR DEM, which were the only data available. Most of the measured faults terminate within the plateau, but some extend to the Novy Semiachik valley in the south, and one fault appears to extend onto the Bolshoi Semiachik caldera scarp (Fig. 7).

Apart from one fault located farther east (dashed line Fig. 7), all other faults are closely spaced and form a graben approximately 8 km wide. There are also numerous fractures expressed by linear rows of sinkholes and depressions within the graben that strike parallel to the fault scarps. The total vertical displacement (approximately 170 m) and graben depth (65 m) indicate that faulting on the plateau is very similar to that on the Shirokoye Plateau (Fig. 8).

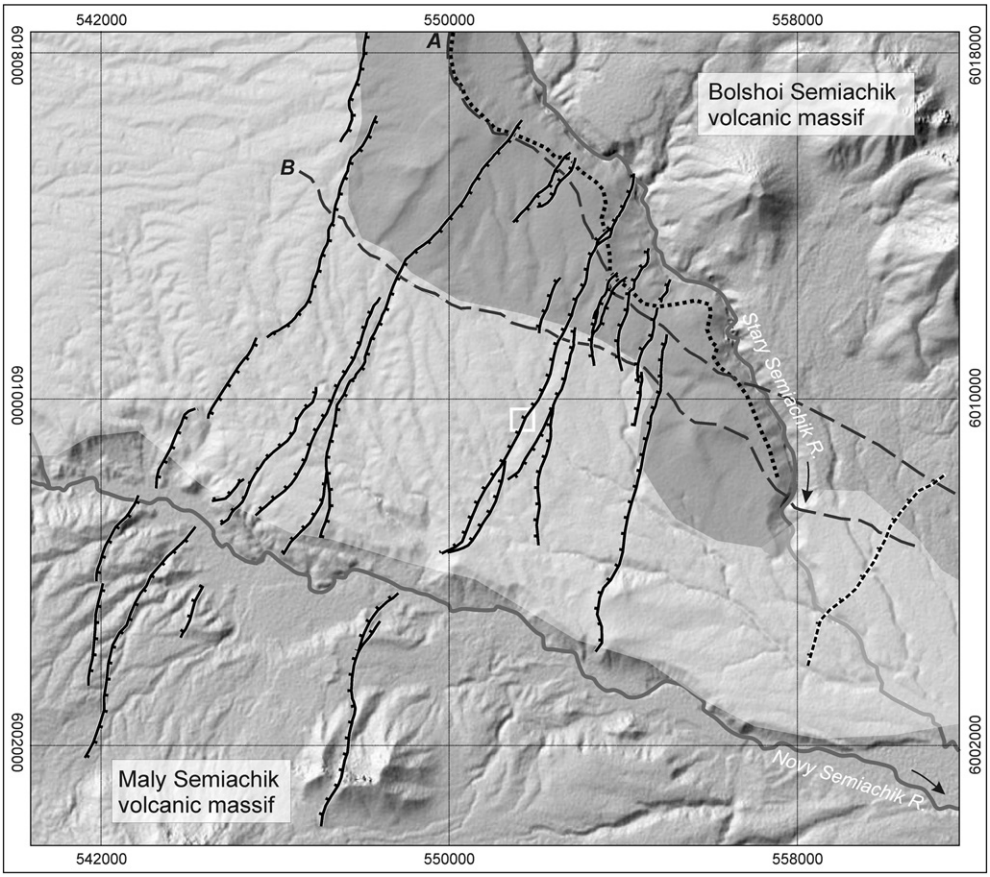

Fig. 7. Normal faults on the Semiachik Plateau. Shaded relief is generated by SRTM X-SAR (©DLR/ASI) data (grid marks in meters). Dashed lines A and B are topographic profiles shown on Fig. 8. White rectangle shows the trench site (Fig. 9). Light grey overlay marks the extent of upper Pleistocene Uzon ignimbrites, dark grey overlay marks middle Pleistocene pre-caldera deposits (Leonov and Grib, 2004).

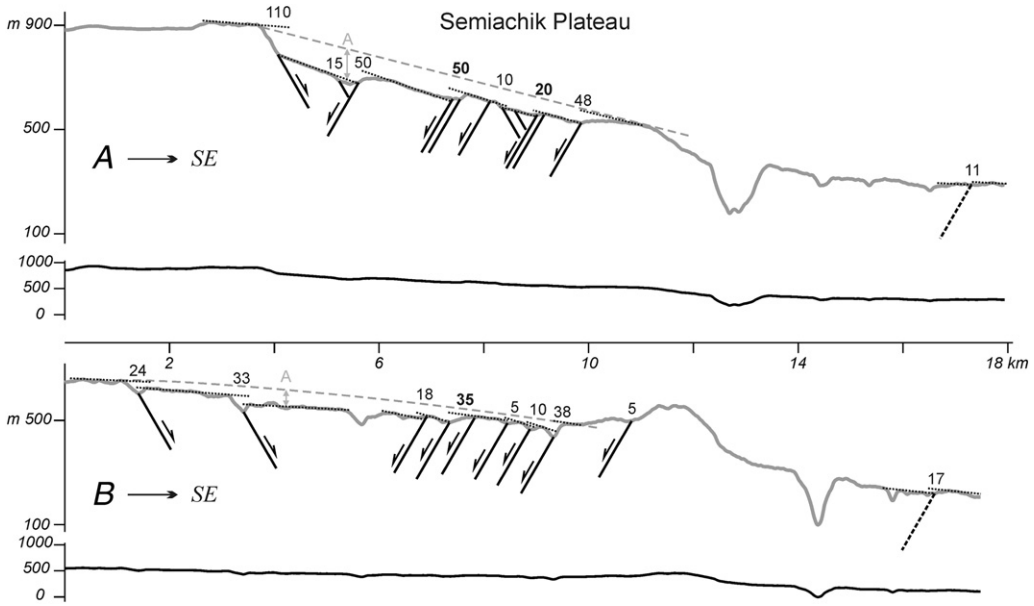

Fig. 8. Hypsometric profiles across the Semiachik Plateau (see Fig. 7 for location), derived from SRTM X-SAR (©DLR/ASI). For symbols, see Fig. 5. Sum of vertical displacements on the faults is approximately 170 m, graben depth is approximately 65 m.

We did not find suitable places on the plateau where fault dips could be measured accurately enough. The only fault exposed in a 2-meter-deep trench that we excavated is normal and dips 70° to the west (Fig. 9) providing the only reference datum for estimating the dip of faults on the Semiachik Plateau.

Because the fault in the trench was accompanied by open fissures in its hanging wall, it may dip somewhat more shallowly below the trench. Due to the lack of direct fault-dip measurements, we assign a fault-dip of 60° degrees that is typical for normal faults in rift-systems globally (Jackson, 1987). With the graben width of 8 km and a total extension of 100 m, we estimate the thickness of the brittle layer to be approximately 7 km.

4. The East Kamchatka fault zone

The structure of the EKFZ varies along strike (Fig. 1). In the north and south, west of the Ganalsky Range and the Kumroch Range, respectively, it comprises individual faults, slip on which accounts for nearly all of the >1 km of topography displacement between the CKD and its eastern flank. In the central region, corresponding to the Valaginsky and Tumrok ranges, the EKFZ splits into numerous individual faults. Thus, the transition from the depression to its elevated flank occurs through a series of blocks with intermediate elevations. In the north, at the latitude of the Kumroch Range, a smaller fault, located ~25 km to the east of the main fault, traverses the landscape (Fig. 1).

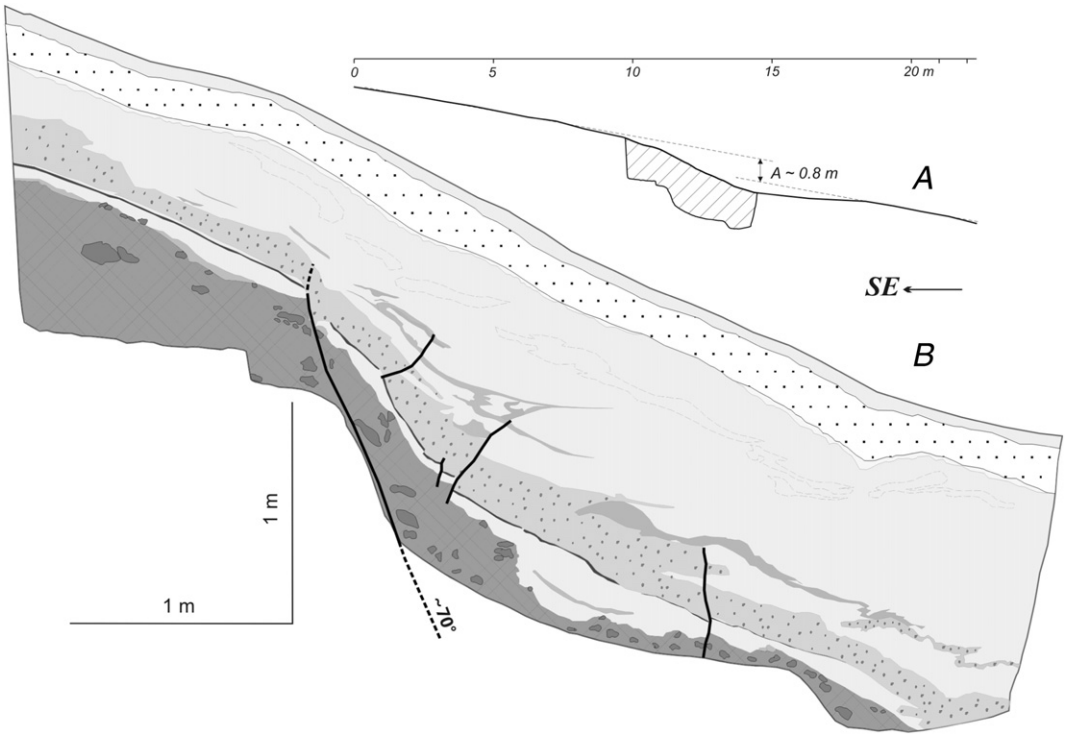

Fig. 9. Log of the Semiachik trench, south wall. For symbols see Fig. 6.

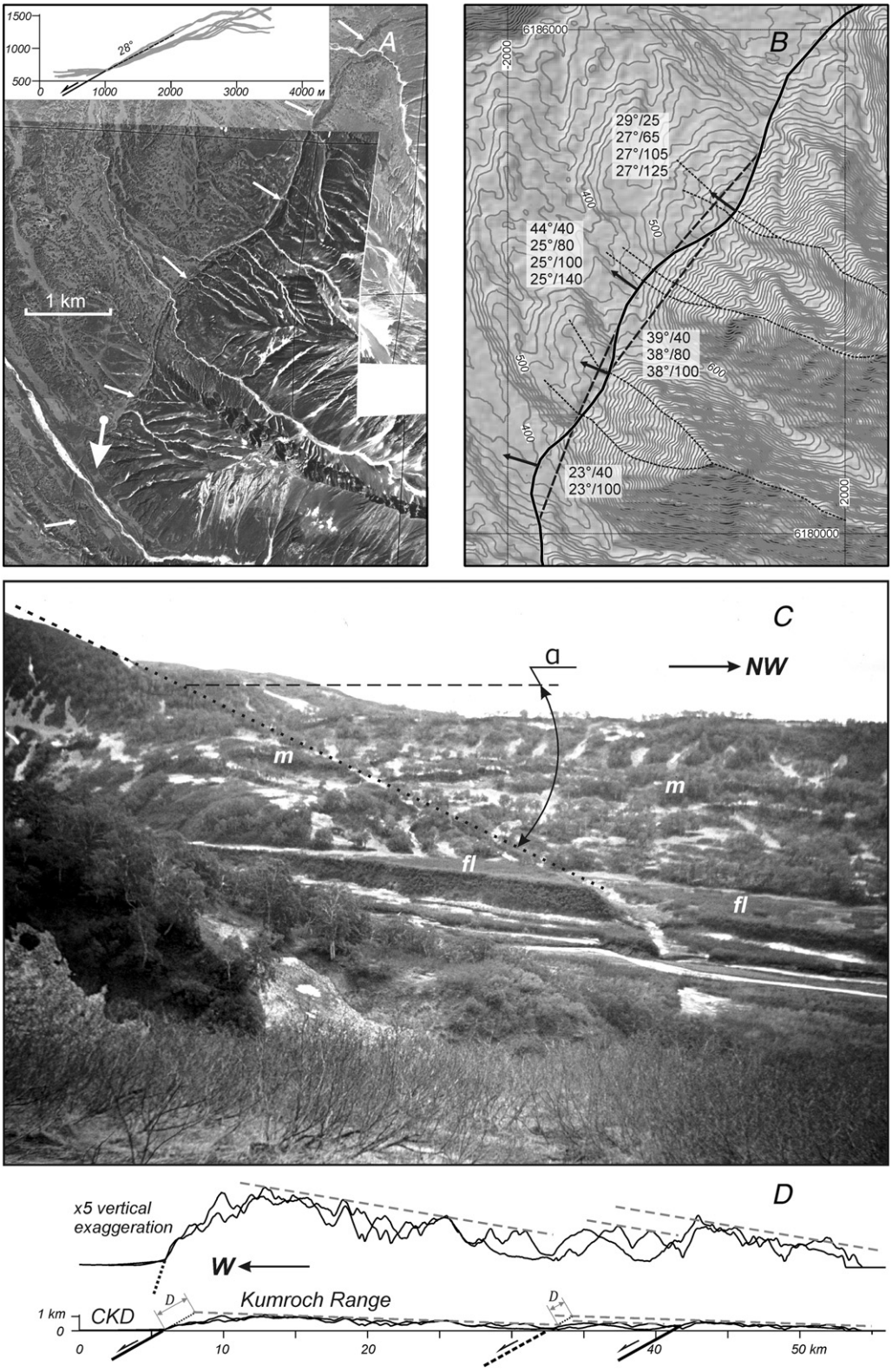

Fig. 10. Normal fault of the Kumroch segment of the EKFZ (see Fig. 1 for location). A is an aerial image, and B is the ASTER GDEM derivative contours and shaded topography of the same scale. White arrows on A point at the fault. Numbers on B are fault dip (left, rounded to 1°) and depth interval it attributes to (right, after slash, see inset on Fig. 4 for determination procedure). Inset on A shows hypsometric profiles (their lines shown in B), yielding 28° as mean value of facet slope angle. C is perspective photograph looking south along the fault. Dotted black line marks the trace of the fault where it cuts upper Pleistocene lateral moraine (m) and fluvioglacial terrace (fl). Photographer is standing right on the fault (see white circle on A, the arrow indicating direction faced), so inclination α, which is ~26°, of the fault trace in the plane of the central part of the picture, where distortion is relatively small, is a good measure of fault dip. Note that, in the image, the facet slopes about the same angle as the fault dips. On D, two of eight profiles (dotted lines on B) demonstrate basic pattern of the range cross-section, with faults dipping at angles measured on B and C. D is the accumulated net offset.

The tops of the elevated blocks are regularly tilted to the east, towards the ocean. The tilting is generally subtle, only a few degrees, but present. Measured by hypsometric profiles, the tilting is 2.9 ± 1.0° (13 measurements) in the Kumroch Range (Fig. 10) and approximately 2.4 ± 1.3° (7 measurements) in the Valaginsky Range (Fig. 11).

Upper Quaternary fluvioglacial and younger fan sediments of the uppermost part of the CKD fill are only slightly incised. Consequently, using the method of mapview fault bends to estimate fault dip is not applicable. The only exception is upper Pleistocene moraine plain, located at the foot of the southern part of Kumroch Range, where glacial valleys are cut by the EKFZ and form slopes up to 200 m in height (Fig. 10). There, 14 measurements of five fault bends yielded dips of 30 ± 6°. The steepest dips of ~39° were measured where strike of the main fault changes from 35 to 40°NE to ~25°NNE. Importantly, the lower-most faceted spurs of the Kumroch Range slope lie at the angle of 28 ± 4°, which is close to that of fault dip measured by fault bends. So the slope angles of the lowermost facets (which are also the steepest) may serve as a proxy for estimating the fault dip with uncertainty of the same magnitude as the direct measurement of fault bends. Notably, in two 2-m-deep trenches excavated across the main fault in this area, the faults were nearly vertical (Kozhurin et al., 2006).

At the latitude of the Shirokoye Plateau, the EKFZ divides the CKD and the Valaginsky Range. To find the dip angle of the EKFZ, we used the bends of two faults within the range and the slope angles of faceted spurs (Fig. 11). The planes of the two faults located within the range dip ~30°, while the slope angles of the faceted spurs fringing the main fault of the EKFZ are 37 ± 6° (average of 8 measurements, see inset to Fig. 11). The hanging wall of the main fault is deformed by a system of longer antithetic and shorter synthetic faults. This may indicate flattening of the fault plane with depth (e.g., Erickson et al., 2001). Nevertheless, to avoid overestimation of the magnitude and the rate of extension across the EKFZ, we chose a dip angle of 37 ± 6° for the master fault plane.

For tilted blocks of the Eastern Ranges between the EKFZ spurs, we obtained a rough estimate of the extension rate using the domino model (planar faults and deformation induced by simple shear in a horizontal plane) and the Thompson formula (Thompson, 1960):

$$E = \sin(\alpha + \beta)/\sin\alpha * 100\%,$$

where α = fault plane dip, β = surface tilt, and E = total extension relative to the width of the initial domain. For the Kumroch Range (α = 30 ± 6°, β = 2.9 ± 1.0°), E = 109 ± 3.7%. Using a total

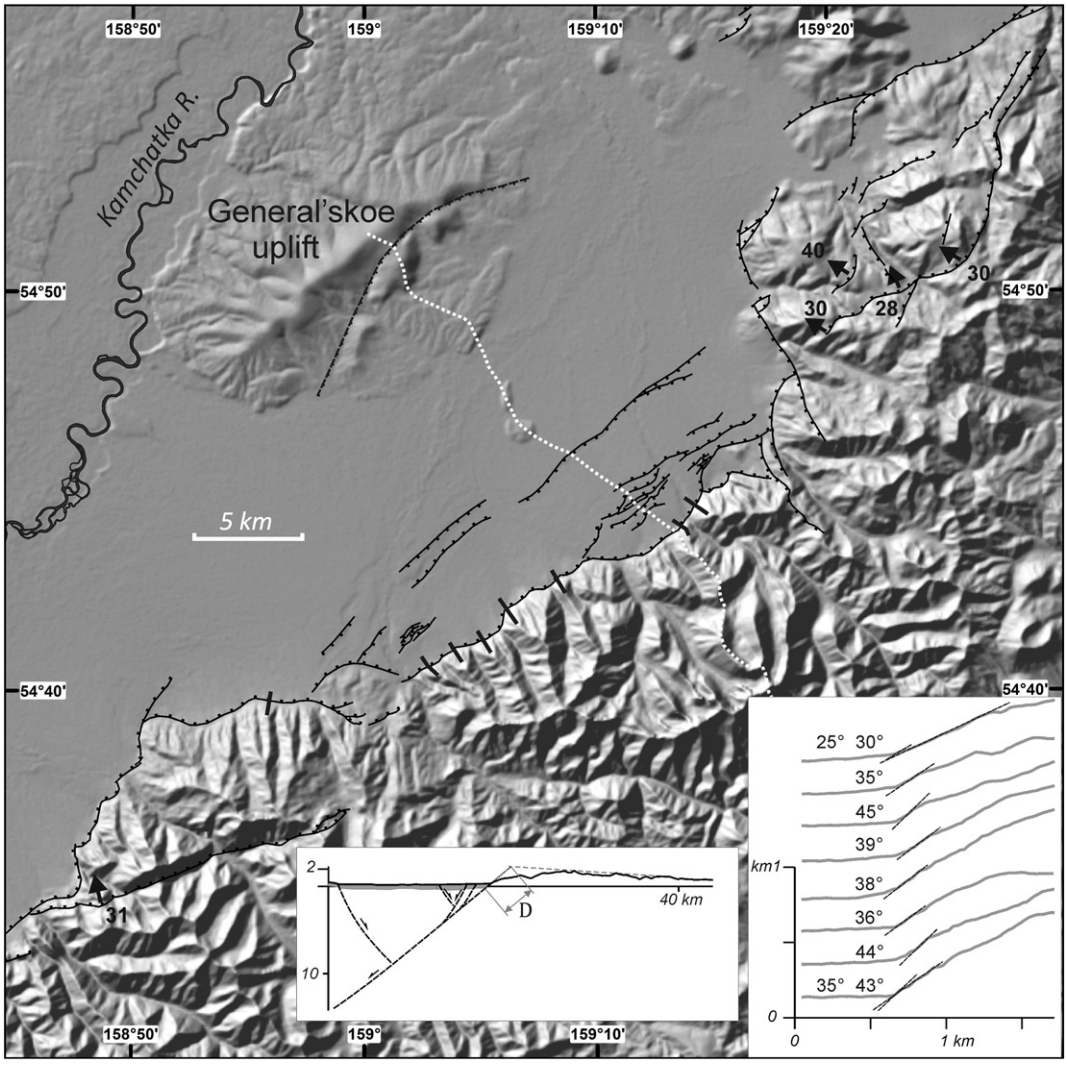

Fig. 11. Normal faults of the Valaginsky segment of the EKFZ (for location see Fig. 1). Black lines are active faults, hatches on downthrown side. Black arrows and digits indicate dip direction and angles found for several subsidiary faults based on their planform geometry. Bottom right inset shows hypsometric profiles of some of faceted spurs (black solid lines) obtained by SRTM X-SAR (©DLR/ASI) data, and their slope angles. Bottom left inset shows principal cross-section of the Valaginsky Range and the EKFZ. Grey-filled areas are CKD sediments, D is accumulated net offset.

deformed area width of 45 km (two blocks, 25 and 20 km wide, see profiles on Fig. 10), we obtained 2.2–5.6 km of horizontal extension, i.e., approximately 2 km for each of the two faults. For the Valaginsky Range ($\alpha = 37 \pm 6°$, $\beta = 2.4 \pm 1.3°$), E = 106 ± 3%. Because the width of the Valaginsky Range block is approximately the same as that of the block between the two faults in the Kumroch Range (~25 km), we obtained approximately 1.5 km of horizontal extension for the one main fault in the Valaginsky Range.

De Matos (1993) noted a high probability of either underestimation of extension for steep faults or overestimation for shallow faults based on the Thompson formula for a domino model. Therefore, De Matos proposed a calculation involving the parameter of inclined simple shear in the hanging wall of a listric fault, a parameter that was not available in our study. Similarly, Poblet and Bulnes (2005) and references within showed that, for listric faults with moderate angles of dip in their upper parts, extension is roughly equal to net displacement of the hanging wall along the fault plane. If this is correct, extension may have reached 2–3.2 km (D on Fig. 10 D) on the main (western) fault in the Kumroch Range and 1–2 km on the eastern fault for a total of 3–5.2 km in the Kumroch Range. These values represent minimum extension estimates because we did not include in our calculation the thickness of the CKD Quaternary fill, which is unknown. At the latitude of the Valaginsky Range, the thickness is approximately 600 m (Braitseva and Melekestsev, 1974), and the displacement along the main fault, together with that expressed topographically (D on bottom left inset in Fig. 11) reaches 3.3–4.9 km, which is close to that estimated for the Kumroch Range.

As we already mentioned above, the growth of the CKD flanks was marked by coarse sediment deposition in the depression, which began in the first half of the middle Pleistocene, during the middle Pleistocene interglacial (Braitseva et al., 1968; Braitseva et al., 2005). During the middle Pleistocene glaciation in Kamchatka, which corresponds to the Samarovo glaciation in Siberia (Braitseva et al., 2005), the Eastern Ranges were already high enough to supply ice flows; thus, the onset of the growth of the Eastern Ranges likely took place close to the transition from the interglacial to the Samara glaciation, from MIS 9 to MIS 8 (Arkhipov, 1989; Astakhov, 2013). As the exact age of sediments in depression remains unknown, both MIS 9e warming around ~330 ka BP, and MIS 9a warming around ~280 ka BP (e.g., Siddall et al., 2007) may be assumed to mark the onset of transition. To cover the uncertainty we attribute part of the lateral extension of Central Kamchatka, accommodated by the EKFZ, to last 300 ± 30 ka, producing an extension rate of 13.7 ± 3.0 mm/yr.

5. Discussion

The rate of arc-normal extension in Central Kamchatka, as our calculations show, may amount to 17.7 ± 3.2 mm/yr. This value relates to only the 200-km-wide onshore part of Central Kamchatka, and does not characterize the extension of the whole arc crust because there is also another 200-km-wide underwater portion of the island arc between the eastern shoreline of Kamchatka and the trench, some part of which may also undergo extension. The underwater slope is structurally differentiated, with the most prominent structures being three sedimentary basins in front of the three bays of the eastern Kamchatka coast, which includes the Avachinsky Bay, the Kronotsky Bay, and the Kamchatcky Bay (Seliverstov, 1998) (Fig. 1). Based on seismic sounding, Seliverstov (1998) concluded that all three basins

Fig. 12. M ≥ 3.5 shallow, <35 km, non-subduction seismicity in Kamchatka from 1962 to 2014 by Geophysical Survey of RAS, Kamchatka branch (www.emsd.ru/sdis/). Solid lines are active faults (simplified, see also Fig. 1), dashed line is approximate SE-limit of diffuse seismicity (except E-W band of earthquakes of unknown structural origin). Note that this limit, although approximate, is located NW of the EKFZ.

evolved synsedimentary, and that rapid submergence of the continental slope took place between the end of early Quaternary and the beginning of the middle Quaternary. Some seismic profiles reveal normal NW-dipping faults along the ocean limits of the basins, resembling normal NW-dipping Central Kamchatka faults.

The absence of central depression, similar to CKD, in South Kamchatka suggests that arc-normal extension south of Central Kamchatka decreases significantly. This may account for the absence of axial grabens in the South Kamchatka volcanic belt, south of Central Kamchatka, and suggest in turn that the arc-normal extension of Central Kamchatka is essential and necessary for the East Volcanic Front to extend by brittle failure. Most likely, rupture of the upper crust in the East Volcanic Front occurs because the brittle layer in the axis of the volcanic belt, where heat flow is highest, is relatively thin (2 to 3 km beneath the Shirokoye Plateau and <10 km beneath the Semiachik Plateau). The thin crust may also account for the small (cm-scale) individual displacements observed in the trenches (Fig. 6), i.e., faults are short and shallow, and therefore, cannot accumulate enough energy to produce larger offsets. The fact that the crust along the Kamchatka island arc breaks where it is thinner implies that faulting in the East Volcanic Front is driven by tectonics (arc-normal extension) and does not result from a ground expression of a "magma supplying channel" or from tearing of the crust by rising magma.

From the hypocentral microearthquakes (M < 5) distribution in Central Kamchatka (Gordeev et al., 2006), the brittle crust beneath the CKD must be 20–25 km thick. Epicenters of these earthquakes form several diffuse bands located 10–15 km west of the EKFZ (Fig. 12), and may result from slip on the deeper section (10–20 km) of gently dipping normal faults of the EKFZ.

6. Conclusions

1. During the middle-late Quaternary, onshore Central Kamchatka has extended at a rather rapid rate of 17 ± 3.2 mm/yr, of which 4.0 ± 1.2 mm/yr is accommodated by extension in the East Volcanic Front. That the offshore extension (that is not calculated in this article) may add up to ~28 mm/yr obtained by Schellart et al. (2007) using numerical modelling of slab-arc motion, supports trench retreat as a driving mechanism of the Central Kamchatka extension.
2. Volcano-tectonic faulting in Central Kamchatka appears to result from superposition of regional ocean-directed lateral extension of a thinned brittle layer in the volcanic belt. The resulting structural patterns, including parallel normal faults and nested grabens, are very similar to those in totally different geodynamic settings, such as in Iceland or the Afar region.

Acknowledgements

The research was supported by grant 16-05-00090 from the Russian Foundation for Basic Research (RFBR) to Kozhurin. The authors are grateful to Vera Ponomareva (Institute of Volcanology and Seismology, Russian Academy of Sciences), without whose assistance and financial support (RFBR grant 06-05-64960) trenching studies on both plateaus would not have been possible. We also thank Vasiliki Mouslopoulou and Alessandro Tibaldi for their helpful and careful reviews of our manuscript.

References

Acocella, V., Funiciello, F., 2010. Kinematic setting and structural control of arc volcanism. Earth Planet. Sci. Lett. 289 (1):43–53. http://dx.doi.org/10.1016/j.epsl.2009.10.027.
Arkhipov, S.A., 1989. A Chronostratigraphic Scale of the Glacial Pleistocene of the West Siberian North. Pleistotsen Sibiri. Stratigrafia i mezhregionalnye korrelatsii. Nauka, Novosibirsk. pp. 20–30 (in Russian).
Astakhov, V.I., 2013. Pleistocene glaciations of northern Russia–a modern view. Boreas 42 (1):1–24. http://dx.doi.org/10.1111/j.1502-3885.2012.00269.x.
Begg, J.G., Mouslopoulou, V., 2010. Analysis of late Holocene faulting within an active rift using lidar, Taupo Rift, New Zealand. J. Volcanol. Geotherm. Res. 190 (1), 152–167.
Bindeman, I.N., Leonov, V.L., Izbekov, P.E., Ponomareva, V.V., Watts, K.E., Shipley, N.K., Perepelov, A.B., Bazanova, L.I., Jicha, B.R., Singer, B.S., Schmitt, A.K., Portnyagin, M.V., Chen, C.H., 2010. Large-volume silicic volcanism in Kamchatka: Ar–Ar and U–Pb ages, isotopic, and geochemical characteristics of major pre-Holocene caldera-forming eruptions. J. Volcanol. Geotherm. Res. 189 (1):57–80. http://dx.doi.org/10.1016/j.jvolgeores.2009.10.009.
Braitseva, O.A., Melekestsev, I.V., 1974. Accumulative plains in the Central Kamchatka depression. History of Relief Development in Siberia and Far East. Kamchatka, the Kuril and Komandor Islands, pp. 234–249 (in Russian).
Braitseva, O.A., Melekestsev, I.V., Evteeva, I.S., Lupikina, E.G., 1968. Stratigraphy of Quaternary Deposits and Glaciations of Kamchatka. Akademia Nauk SSSR, Moscow (in Russian).
Braitseva, O.A., Melekestsev, I.V., Sulerzhitsky, L.D., 2005. New data on the Pleistocene deposits in the Central Kamchatka Depression. Stratigr. Geol. Correl. 13 (1), 99–107.
Bronk Ramsey, C., 2009. Bayesian analysis of radiocarbon dates. Radiocarbon 51 (01), 337–360.
Erickson, S.G., Strayer, L.M., Suppe, J., 2001. Mechanics of extension and inversion in the hanging walls of listric normal faults. J. Geophys. Res. 106 (11), 26,655–26,670.
Fitch, T.J., 1972. Plate convergence, transcurrent faults, and internal deformation adjacent to southeast Asia and the western Pacific. J. Geophys. Res. 77 (23), 4432–4460.
Florensky, I.V., 1984. On the age of Uzon and Krashenninnikov calderas. J. Volcanol. Seismol. 1, 102–106 (in Russian).
Florensky, I.V., Trifonov, V.G., 1985. Neotectonics and volcanism of the east volcanic zone of Kamchatka. Geotektonika 4, 78–87 (In Russian).
Giba, M., Nicol, A., Walsh, J.J., 2010. Evolution of faulting and volcanism in a back-arc basin and its implications for subduction processes. Tectonics 29 (4).
Gordeev, E.I., Gusev, A.A., Levina, V.I., Leonov, V.L., Chebrov, V.N., 2006. Shallow earthquakes in the Kamchatka Peninsula. J. Volcanol. Seismol. 3, 40–55.
Jackson, J.A., 1987. Active normal faulting and crustal extension. Geol. Soc. Lond., Spec. Publ. 28 (1), 3–17.
Kozhurin, A., Acocella, V., Kyle, P.R., Lagmay, F.M., Melekestsev, I.V., Ponomareva, V., Rust, D., Tibaldi, A., Tunesi, A., Corazzato, C., Rovida, A., Sakharov, A., Tengonciang, A., Uy, H., 2006. Trenching studies of active faults in Kamchatka, eastern Russia: palaeoseismic, tectonic and hazard implications. Tectonophysics 417 (3), 285–304.
Kozhurin, A.I., Pinegina, T.K., Ponomareva, V.V., Zelenin, E.A., Mikhailyukova, P.G., 2014. Rate of collisional deformation in Kamchatsky Peninsula, Kamchatka. Geotectonics 48 (2), 122–138.
Lander, A.V., Shapiro, M.N., 2007. The Origin of the Modern Kamchatka Subduction Zone. Volcanism and Subduction, The Kamchatka Region, pp. 57–64.
Legler, V.A., Parfenov, L.M., 1979. Fault systems in island arcs. Tectonic Zoning and Structural-formation Evolution of NE Asia, pp. 134–156 (in Russian).
Leonov, V.L., Grib, E.N., 2004. The Structural Position and Volcanism of the Quaternary Calderas, Kamchatka Russia. Dal'nauka, Vladivostok (in Russian).
de Matos, R.M.D., 1993. Geometry of the hanging wall above a system of listric normal faults - a numerical solution. AAPG Bull. 77 (11), 1839–1859.
Mouslopoulou, V., Nicol, A., Walsh, J.J., Begg, J.G., Townsend, D.B., Hristopulos, D.T., 2012. Fault-slip accumulation in an active rift over thousands to millions of years and the importance of paleoearthquake sampling. J. Struct. Geol. 36, 71–80.
Nicol, A., Walsh, J., Berryman, K., Villamor, P., 2006. Interdependence of fault displacement rates and paleoearthquakes in an active rift. Geology 34 (10), 865–868.
Poblet, J., Bulnes, M., 2005. Fault-slip, bed-length and area variations in experimental roll-over anticlines over listric normal faults: influence in extension and depth to detachment estimations. Tectonophysics 396 (1), 97–117.
Ponomareva, V.V., Churikova, T.G., Melekestsev, I.V., Braitseva, O.A., Pevzner, M.M., Ponomareva, V., Melekestsev, I., Braitseva, O., Churikova, T., Pevzner, M., Sulerzhitsky, L., 2007. Late Pleistocene-Holocene Volcanism on the Kamchatka Peninsula, Northwest Pacific Region. Volcanism and Subduction, The Kamchatka Region, pp. 165–198.
Rabinovich, S.G., 2006. Measurement Errors and Uncertainties: Theory and Practice. Springer Science & Business Media.
Reimer, P.J., Bard, E., Bayliss, A., Beck, J.W., Blackwell, P.G., Ramsey, C.B., Buck, C.E., Cheng, H., Edwards, R.L., Friedrich, M., Grootes, P.M., Guilderson, T.P., Haflidason, H., Hajdas, I., Hatte, C., Heaton, T.J., Hoffmann, D.L., Hogg, A.G., Hughen, K.A., Kaiser, K.F., Kromer, B., Manning, S.W., Niu, M., Reimer, R.W., Richards, D.A., Scott, E.M., Southon, J.R., Staff, R.A., Turney, C.S.M., van der Plicht, J., 2013. IntCal13 and Marine13 radiocarbon age calibration curves 0–50,000 years cal BP. Radiocarbon 55 (4), 1869–1887.0.
Schellart, W.P., Freeman, J., Stegman, D.R., Moresi, L., May, D., 2007. Evolution and diversity of subduction zones controlled by slab width. Nature 446 (7133), 308–311.
Schellart, W.P., Stegman, D.R., Freeman, J., 2008. Global trench migration velocities and slab migration induced upper mantle volume fluxes: constraints to find an Earth reference frame based on minimizing viscous dissipation. Earth Sci. Rev. 88 (1), 118–144.
Seliverstov, N.I., 1998. The Kamchatka Offshore and Geodynamics of the Kuriles-Kamchatka and the Aleutian Junction. Nauchnyi Mir, Moscow (in Russian).
Seliverstov, N.I., 2009. Geodynamics of the Kuriles-Kamchatka – Aleutian Junction. KamGU im, Vitusa Beringa (in Russian).
Shantser, A.E., 1979. Some peculiarities in evolution of tectono-magmatic structures in Kamchatka as reflecting its block structure and blocks movements in Late Cenozoic. Bulletin of Volcanoligical. Station of Academy of Sciences of USSR. 57, pp. 54–65 (in Russian).
Siddall, M., Chappell, J., Potter, E.K., 2007. 7. Eustatic sea level during past interglacials. Developments in Quaternary Sciences. 7, pp. 75–92.
Thompson, G.A., 1960. Problem of late Cenozoic structure of the Basin Ranges. International Geological Congress, XXI Session, Part XVIII, pp. 62–68.
Villamor, P., Berryman, K., 2001. A late Quaternary extension rate in the Taupo Volcanic Zone, New Zealand, derived from fault slip data. N. Z. J. Geol. Geophys. 44 (2), 243–269.